

GRB 221009A afterglow from a shallow angular structured jet

Ramandeep Gill^{1,2★} and Jonathan Granot^{2,3,4★}

¹*Instituto de Radioastronomía y Astrofísica, Universidad Nacional Autónoma de México, Antigua Carretera a Pátzcuaro # 8701, Ex-Hda. San José de la Huerta, Morelia, Michoacán, México C.P. 58089, México*

²*Astrophysics Research Center of the Open University (ARCO), The Open University of Israel, P.O. Box 808, Ra'anana 4353701, Israel*

³*Department of Natural Sciences, The Open University of Israel, P.O. Box 808, Ra'anana 4353701, Israel*

⁴*Department of Physics, The George Washington University, Washington, DC 20052, USA*

Accepted 2023 June 8. Received 2023 June 5; in original form 2023 April 28

ABSTRACT

Exceptionally bright gamma-ray burst (GRB) afterglows can reveal the angular structure of their jets. GRB jets appear to have a narrow core (of half-opening angle θ_c), beyond which their kinetic energy drops as a power-law with angle θ from the jet's symmetry axis, $E_{k, \text{iso}}(\theta) \propto [1 + (\theta/\theta_c)^2]^{-a/2}$. The power-law index a reflects the amount of mixing between the shocked jet and confining medium, which depends on the jet's initial magnetization. Weakly magnetized jets undergo significant mixing, leading to shallow ($a \lesssim 2$) angular profiles. We use the exquisite multiwaveband afterglow observations of GRB 221009A to constrain the jet angular structure using a dynamical model that accounts for both the forward and reverse shocks, for a power-law external density profile, $n_{\text{ext}} \propto R^{-k}$. Both the forward shock emission, that dominates the optical and X-ray flux, and the reverse shock emission, that produces the radio afterglow, require a jet with a narrow core ($\theta_c \approx 0.021$) and a shallow angular structure ($a \approx 0.8$) expanding into a stellar wind ($k \approx 2$). Moreover, these data appear to favour a small fraction ($\xi_e \approx 10^{-2}$) of shock heated electrons forming a power-law energy distribution in both shocks.

Key words: relativistic processes – gamma-ray burst: general – stars: jets.

1 INTRODUCTION

New paradigm-shifting insights into gamma-ray burst (GRB) physics can be gained by observing exceptionally bright GRBs, such as the recent GRB 221009A (An et al. 2023; Burns et al. 2023; Frederiks et al. 2023; Lesage et al. 2023; Ripa et al. 2023) that had an extremely high fluence of $S_\gamma \sim 0.2 \text{ erg cm}^{-2}$. This is a result of its relatively closer distance, with a redshift of $z = 0.151$ (e.g. de Ugarte Postigo et al. 2022; Malesani et al. 2023), and a record-breaking prompt γ -ray isotropic equivalent energy release of $E_{\gamma, \text{iso}} \sim 1.2 \times 10^{55} \text{ erg}$, over a total duration of $t_{\text{GRB}} \sim 600 \text{ s}$. This GRB is even more important and unique since the Large High Altitude Air Shower Observatory (LHAASO) reported the detection of over 5000 very high-energy photons, including an 18 TeV photon, within 2000 s of the burst trigger (Huang et al. 2022).

The broad-band afterglow of this burst was recorded in exquisite detail from radio to γ -rays (An et al. 2023; Bright et al. 2023; Frederiks et al. 2023; Fulton et al. 2023; Kann et al. 2023; Laskar et al. 2023; Lesage et al. 2023; O'Connor et al. 2023; Williams et al. 2023). Its modelling in some of these works and others (Ren et al. 2022; Sato et al. 2023) with the canonical forward shock (FS) and reverse shock (RS) emission from a uniform and even a two-component jet presented some challenges. In particular, Laskar et al. (2023) found it difficult to explain the radio data both with the RS and FS afterglows in the wind ($k = 2$) scenario (for an external medium density $n_{\text{ext}} \propto R^{-k}$) which they preferred over the interstellar medium

(ISM; $k = 0$) case. In addition, their FS model could not adequately fit both the early- ($\lesssim 1 \text{ d}$) and late-time ($\gtrsim 30 \text{ d}$) optical data. Some success was achieved by O'Connor et al. (2023) who modelled the FS emission from a shallow angular structured jet and the RS emission from a spherical outflow expanding into a uniform medium (ISM).

The angular structure of the relativistic outflows in GRBs is challenging to constrain. An important step in this direction came with the discovery of the coincident detection of gravitational waves and short prompt GRB emission from the binary neutron star merger in GW170817 (Abbott et al. 2017), followed by a peculiar afterglow (e.g. Margutti et al. 2018; Troja et al. 2019). Hints of jet angular structure were also found in other GRBs (e.g. Racusin et al. 2008). An angular structure naturally forms as the jet bores its way through the confining medium near its launching site, i.e. the stellar envelope in long-soft GRBs and the binary merger ejecta in short-hard GRBs, as has been demonstrated with numerical simulations (e.g. Gottlieb et al. 2020; Gottlieb, Nakar & Bromberg 2021; Nathanail et al. 2021). More importantly, the jet angular structure is sensitive to the amount of mixing that occurs during jet breakout, between the inner and outer cocoon (shocked jet material and confining medium). The amount of mixing is, in turn, strongly affected by the jet's initial magnetization, which remains poorly constrained and its knowledge is of paramount importance.

Afterglow emission arising from the FS for different jet angular structures have been calculated in several works (e.g. Rossi, Lazzati & Rees 2002; Granot & Kumar 2003; Kumar & Granot 2003; Rossi et al. 2004; Granot 2005; Granot, Ramirez-Ruiz & Perna 2005; Gill & Granot 2018, 2020; Beniamini, Granot & Gill 2020, 2022) with varying degree of sophistication. The RS emission from such

* E-mail: rsgill.rg@gmail.com (RG); granot@openu.ac.il (JG)

jets with angular structure was considered only in few works (Yan, Wei & Fan 2007; Lamb & Kobayashi 2019). Here, we systematically consider the RS emission from jets with angular structure, along with the system's global RS–FS dynamics, which becomes important in the thick-shell regime (see Section 2).

The multiwaveband afterglow observations of the exceptionally bright GRB 221009A present a golden opportunity to constrain the jet angular structure and its initial magnetization. We start by summarizing the analytic scalings for thin and thick shells in Section 2 for later comparison. In Section 3, we calculate the FS and RS dynamical evolution in an adiabatic spherical blast wave using our semi-analytical model. We extend this model to angular structured jets and obtain the afterglow emission from both shocks in Section 4. By comparing the emission to time-resolved spectra and light curve of GRB 221009A, we demonstrate that its afterglow is produced by a jet with a shallow angular structure. The implications of our results are discussed in Section 5.

2 FORWARD–REVERSE SHOCK DYNAMICS

The self-similar dynamical evolution and radial structure of a relativistic spherical blast wave was first calculated by Blandford & McKee (1976, BM76 hereafter). It was used to explain the long-lasting and broad-band afterglow emission of GRBs in several seminal works (e.g. Rees & Meszaros 1992; Meszaros & Rees 1993; Sari & Piran 1995). In this model, a cold baryonic spherical shell of (lab-frame) initial width Δ_0 and with kinetic energy $E_{k,\text{iso}}$ coasting at an initial bulk-LF Γ_0 is decelerated by sweeping up the surrounding external medium with number density $n_{\text{ext}}(R) = n_0(R/R_0)^{-k}$. In the process, a double shock structure develops with four different regions (quantities in these regions have their respective labels): (1) the unshocked external medium; (2) the shocked external medium; (3) the shocked ejecta; and (4) the unshocked ejecta. Regions 2 and 3 are separated by a contact discontinuity (CD) and thus have the same pressure and LF, $\Gamma_2 = \Gamma_3$. A relativistic FS propagates into region 1 with bulk LF $\Gamma_{\text{sh}} = \sqrt{2}\Gamma_2$, shock heating the swept up external medium and accelerating it to a LF Γ_2 . At the same time, a RS, which may either be relativistic (thick shell) or not (thin shell), propagates into the relativistic ejecta, shock heating, and decelerating it.

The dynamical evolution of this adiabatically expanding system (Sari & Piran 1995; Kobayashi, Piran & Sari 1999) depends on whether the RS becomes relativistic before crossing the ejecta, the so-called thick-shell scenario for which $\Gamma_4 = \Gamma_0 > \Gamma_{\text{cr}}$, or remains Newtonian (or becomes at least mildly relativistic) as in the thin-shell case for which $\Gamma_0 < \Gamma_{\text{cr}}$. The two regimes are separated by the critical LF (e.g. Kobayashi & Zhang 2003; Granot 2012; Granot & Ramirez-Ruiz 2012), $\Gamma_{\text{cr}} = (\ell/\Delta_0)^{(3-k)/2(4-k)}$, where $\ell \equiv (E_{k,\text{iso}}/Ac^2)^{1/(3-k)}$ is the Sedov length (ignoring order unity factors), $A = m_p n_0 R_0^k$, and m_p is the proton mass. The initial width of the shell can be inferred from $\Delta_0 = (1+z)^{-1} ct_{\text{GRB}}$ for a prompt GRB of apparent duration t_{GRB} at a redshift z .

After the RS becomes relativistic in the thick-shell case, it starts to considerably reduce the ejecta's bulk LF ($\Gamma_3 \ll \Gamma_4$). During this time, the LF of the shocked material (contact discontinuity) is independent of Γ_0 and obeys the scaling $\Gamma_3 = \Gamma_2 \sim (L/Ac^3)^{1/4} R^{-(2-k)/4}$ (Sari 1997) where $L = E_{k,\text{iso}}c/\Delta_0$ is the source's (isotropic equivalent) kinetic power. After that, only a small fraction of the initial kinetic energy of the ejecta is extracted at a radius where the mass of the swept up external medium becomes comparable to M_0/Γ_0 , with $M_0 = E_{k,\text{iso}}/\Gamma_0 c^2$ being the baryon load of the ejecta. Most of this energy is extracted at the shock crossing radius, $R_\Delta \sim R_{\text{cr}} \sim \Delta_0 \Gamma_{\text{cr}}^2$, where the shocked ejecta and shocked external medium have com-

parable energies. Beyond R_{cr} , most of the initial kinetic energy of the ejecta resides in the shocked external medium while the fraction in the shocked ejecta rapidly declines. The evolution of the blast wave (FS) is then described by the self-similar BM76 solution such that $\Gamma_2 \sim \Gamma_{\text{cr}}(R/R_{\text{cr}})^{-(3-k)/2} \sim (E_{k,\text{iso}}/Ac^2)^{1/2} R^{-(3-k)/2}$. So long the shocked ejecta is relativistically hot (with adiabatic index $\hat{\gamma} = 4/3$), its evolution is approximately consistent with the BM76 self-similar radial profile (Kobayashi et al. 1999; Sari & Piran 1999a, b; Kobayashi & Sari 2000), with $\Gamma_3 \sim \Gamma_{\text{cr}}(R/R_{\text{cr}})^{-(7-2k)/2}$. When the temperature of the shocked ejecta becomes non-relativistic, the BM76 solution no longer applies to it.

In the thin-shell case, the RS never becomes relativistic. It is initially Newtonian and for a reasonable spread in the initial LF, $\Delta\Gamma_0 \sim \Gamma_0$, it starts spreading radially at $R_s \sim \Delta_0 \Gamma_0^2$ with $\Delta \sim \max(\Delta_0, R/\Gamma_0^2)$, and becomes mildly relativistic near the crossing radius, $R_\Gamma \sim (E_{k,\text{iso}}/Ac^2 \Gamma_0^2)^{1/(3-k)} \sim \ell \Gamma_0^{-2/(3-k)}$. Therefore, at R_Γ we have $\Gamma_3 = \Gamma_2 \approx \Gamma_0$, the swept up mass is $\sim M_0/\Gamma_0$, and most of the kinetic energy is transferred to the shocked external medium. Beyond R_Γ the blast wave (FS) commences the BM76 self-similar evolution. Since, the RS never becomes relativistic, the shocked ejecta remains at a sub-relativistic temperature (with $\hat{\gamma} = 5/3$). As a result, its evolution cannot be described by the BM76 solution after shock crossing. Assuming a power-law with $\Gamma_3(R) \propto R^{-g}$, Kobayashi & Sari (2000) argued that $3/2 \leq g \leq 7/2$ (or $\frac{3-k}{2} \leq g \leq \frac{7-2k}{2}$ for a general k) and showed that $g \sim 2$ is consistent with one-dimensional hydrodynamical numerical simulations.

3 ADIABATIC SPHERICAL BLAST WAVES

Many works have considered the dynamical evolution of an impulsive relativistic blast wave undergoing adiabatic and/or radiative expansion (Blandford & McKee 1976; Katz & Piran 1997; Chiang & Dermer 1999; Huang, Dai & Lu 1999; Piran 1999; Beloborodov & Uhm 2006; Pe'er 2012) mostly in the limit of a homogeneous shell where its radial structure is ignored. Most of these works have focused on the thin-shell scenario where the RS contribution to the system dynamics is relatively modest. However, including the influence of the RS on the system dynamics is crucial in the thick shell case, which is most relevant for many long GRBs, and makes the model more realistic in the thin-shell case. Here, we adopt the self-consistent model of Nava et al. (2013) (also see Zhang et al. 2022) that treats the entire dynamical evolution of an adiabatic/radiative blast wave and allows for an arbitrary density profile of the external medium. Below, we only present its most salient features.

Consider a relativistic spherical shell of initial (lab-frame) thickness Δ_0 , bulk LF Γ_0 , and mass-loading M_0 expanding into an external medium with number density $n_{\text{ext}}(R)$. The (lab-frame) total energy of the system is $E_{\text{tot}} = \Gamma_0 M_{0,4} c^2 + \Gamma M_{0,3} c^2 + \Gamma m c^2 + \Gamma_{\text{eff},3} E'_{\text{int},3} + \Gamma_{\text{eff},2} E'_{\text{int},2}$ where $\Gamma_4 = \Gamma_0$ and $M_0 = M_{0,3} + M_{0,4}$. During RS crossing, it is assumed that both regions (2) and (3) are in pressure balance ($P'_2 = P'_3$) and move with the same bulk LF ($\Gamma_3 = \Gamma_2 \equiv \Gamma$). The total mass swept up by the blast wave as it propagates a radial distance R in an external medium with density $n_{\text{ext}}(R) \propto R^{-k}$ is $m(R) = [4\pi m_p / (3-k)] R^3 n_{\text{ext}}(R)$ for $k < 3$. The comoving internal energy of the shocked material is given by E'_{int} and $\Gamma_{\text{eff}} = (\hat{\gamma}\Gamma^2 - \hat{\gamma} + 1)/\Gamma$ is the appropriate LF to accurately describe the Lorentz transformation of the internal energy (Pe'er 2012). Here, $\hat{\gamma} = (4\Gamma_{\text{ud}} + 1)/3\Gamma_{\text{ud}} = 4/3(5/3)$ is the adiabatic index for a fluid with relativistic (non-relativistic) temperature and $\Gamma_{\text{ud}} = \Gamma_u \Gamma_d (1 - \beta_u \beta_d)$ is the relative LF between the upstream and downstream material that have LFs $\Gamma_{\{u,d\}} = (1 - \beta_{\{u,d\}}^2)^{-1/2}$.

As the shell propagates an infinitesimal radial distance dR , its total energy changes by an amount $dE_{\text{tot}} = dmc^2 + \Gamma_{\text{eff},2} dE'_{\text{rad}}$ that is a sum of the rest-mass energy of the matter swept up over that interval, $dm = 4\pi m_p R^2 n_{\text{ext}} dR$, and the energy that is radiated away. For an adiabatic blast wave, radiative losses are negligible over the dynamical time, and therefore, the second term can be neglected. The change in the internal energy of the shocked material is a sum of three terms, $dE'_{\text{int}} = dE'_{\text{sh}} + dE'_{\text{ad}} + dE'_{\text{rad}}$. Here, $dE'_{\text{sh}} = (\Gamma_{\text{ud}} - 1)dMc^2$ is the random kinetic energy of the newly shocked material, where $dM = dm$ for region (2) and $dM = dM_{0,3}$ for region (3). The terms dE'_{ad} and dE'_{rad} represent the change in energy due to adiabatic and radiative losses (see equation 13 of Nava et al. 2013). By taking the differential of E_{tot} and noticing that $dM_{0,4} = -dM_{0,3}$, the rate of change of the bulk LF of the shocked material can be obtained,

$$\frac{d\Gamma}{dR} = -\frac{(\Gamma_{\text{eff},2} + 1)(\Gamma - 1)\frac{dm}{dR}c^2 + \Gamma_{\text{eff},2}\frac{dE'_{\text{ad},2}}{dR}}{(M_{0,3} + m)c^2 + E'_{\text{int},2}\frac{d\Gamma_{\text{eff},2}}{dR} + E'_{\text{int},3}\frac{d\Gamma_{\text{eff},3}}{dR}} - \frac{(\Gamma - \Gamma_0 - \Gamma_{\text{eff},3} + \Gamma_{\text{eff},3}\Gamma_{43})\frac{dM_{0,3}}{dR}c^2 + \Gamma_{\text{eff},3}\frac{dE'_{\text{ad},3}}{dR}}{(M_{0,3} + m)c^2 + E'_{\text{int},2}\frac{d\Gamma_{\text{eff},2}}{dR} + E'_{\text{int},3}\frac{d\Gamma_{\text{eff},3}}{dR}}. \quad (1)$$

This equation needs to be supplemented by $dM_{0,3}/dR$, the rate at which ejecta mass is entering the RS. The differential number of baryons shocked by the RS as it moves a (lab-frame) radial distance $d\Delta$ into the ejecta is $dN_4 = 4\pi R^2 n'_4 \Gamma_4 d\Delta$. Here, we explicitly assume that the width of the shocked region is much smaller than the radial distance of the blast wave, and therefore, both shocks are approximately at the same radius, such that $R_{\text{RS}} \sim R_{\text{FS}} = R$. Conservation of baryon number dictates that $d\Delta = (\beta_4 - \beta_3)(1 - \Gamma_4 n'_4 / \Gamma_3 n'_3)^{-1} dR$ (Sari & Piran 1995). Putting this all together yields the mass injection rate into region (3), $dM_{0,3}/dR = 4\pi R^2 \rho'_4 \Gamma_0 (\beta_0 - \beta) (1 - \Gamma_0 \rho'_4 / \Gamma_0 \rho'_3)^{-1}$, where $\rho'_4 = M_0 / 4\pi R^2 \Delta \Gamma_0$ is the proper mass density of the ejecta shell that has lab-frame width $\Delta = \max[\Delta_0, R / \Gamma_0^2]$.

We solve the system of equations describing $d\Gamma/dR$ and $dM_{0,3}/dR$ using a fourth-order Runge–Kutta–Fehlberg (RK45) routine with adaptive step size. Until RS crossing $\Gamma_3(R) = \Gamma_2(R) = \Gamma(R)$, but after RS crossing the evolution of the shocked ejecta is prescribed to either have a BM76 profile (thick-shell), with $u_3(R) = \Gamma_3(R)\beta_3(R) = u_\Delta(R/R_\Delta)^{-(7-2k)/2}$, or a general power-law (thin-shell), with $u_3(R) = u_\Delta(R/R_\Delta)^{-s}$. The shock crossing radius (R_Δ) is determined by integrating the equation for $dM_{0,3}/dR$ and by implementing the condition $M_{0,3}(R_\Delta) = M_0$, and the corresponding $u_\Delta = u(R_\Delta)$ is obtained from the solution of equation (1).

The BM76 profile is strictly valid for a relativistically hot gas that has adiabatic index $\hat{\gamma} = 4/3$. As the flow expands, the comoving pressure and number density decline as $P'_3 \propto R^{-2(13-2k)/3}$ and $n'_3 \propto R^{-(13-2k)/2}$. The sound speed in the comoving frame, $c'_s/c = (\hat{\gamma} P'/w')^{1/2}$, depends on the ratio $w'/P' = (\rho'/P')c^2 + \hat{\gamma}/(\hat{\gamma} - 1)$, where w' is the enthalpy density. In the thick-shell case, the shocked gas is initially relativistically hot, which means that $(\rho'_3/P'_3)c^2 \ll \hat{\gamma}/(\hat{\gamma} - 1)$ and therefore, $c'_{s,3}/c = \sqrt{\hat{\gamma}_3 - 1} = 1/\sqrt{3}$. The ratio $\rho'_3/P'_3 \propto R^{(13-2k)/6}$ grows with radius, and as a result, a relativistically hot fluid will become non-relativistic. Therefore, we switch to the thin-shell evolution when $(\rho'_3/P'_3)c^2 > \hat{\gamma}_3/(\hat{\gamma}_3 - 1) = 4$.

In Fig. 1, we show the proper speed $u = \Gamma\beta$ evolution of the shocked material downstream of both the RS and FS for a thin- and thick-shell (left-hand and middle panels) and for different external medium density profiles in the thick shell case (right-hand panel). We compare the asymptotic slopes of $u(R)$ in different regimes with analytical results and find excellent agreement. The model evolves

the bulk LFs of the shocked material downstream of both the shocks until the crossing radius R_Δ and only for the material behind the FS thereafter. For $R > R_\Delta$, the $u_3(R)$ profiles are manually prescribed. In the thick-shell case, $u_3(R)$ shows a change in slope as the shocked material transitions from having a relativistic (thick-shell) to a non-relativistic (thin-shell) temperature.

4 THE AFTERGLOW OF GRB 221009A

We consider an ultra-relativistic outflow with a power-law angular structure to describe the afterglow of GRB 221009A. This type of structure has been obtained in numerical simulations of long (short) GRB jets penetrating out of the progenitor star (merger ejecta; e.g. Gottlieb et al. 2021), and was successful in explaining the peculiar afterglow of GW 170817/GRB 170817A (e.g. Gill & Granot 2018).

Both the energy per unit solid angle, $\epsilon(\theta) = dE(\theta)/d\Omega = E_{k,\text{iso}}(\theta)/4\pi$, where $d\Omega$ is the element of the solid angle, and the initial bulk LF (−1) are described by a power-law at polar angle θ (measured from the jet symmetry axis) larger than some core angle θ_c (e.g. Granot & Kumar 2003)

$$\left\{ \frac{\epsilon}{\epsilon_c}, \frac{\Gamma_0(\theta) - 1}{\Gamma_c - 1} \right\} = \left[1 + \left(\frac{\theta}{\theta_{c, \{\epsilon, \Gamma\}}} \right)^2 \right]^{-\{a, b\}/2}. \quad (2)$$

The core angle and power-law indices for the energy and bulk LF are allowed to be different. Here, we apply our model of a spherical blast wave to an angular structured flow by assuming that every angle θ on the flow’s surface evolves independently as if it were part of a spherical flow with kinetic energy $E_{k,\text{iso}}(\theta)$ and initial LF $\Gamma_0(\theta)$. Its dynamical evolution is obtained by solving the equations used for the spherical flow but now on a grid of polar angles θ . For simplicity and computational convenience we ignore lateral spreading, which becomes important as the outflow approaches the non-relativistic Sedov–Taylor phase. In Fig. 2, we show the angular structure of the outflow that was adopted in order to describe the afterglow of GRB 221009A.

To calculate the afterglow emission we adopt the treatment in Gill & Granot (2018) and assume for simplicity that it arises from an infinitely thin-shell. The two shocks accelerate a fraction ξ_e of the total swept up electrons into a power-law energy distribution with $dn'_e/d\gamma_e \propto \gamma_e^{-p}$ (for $\gamma_e > \gamma_m$), where n'_e is the number density of the synchrotron emitting electrons and γ_e is their LF. These electrons receive a fraction ϵ_e of the total internal energy of the shocked gas, whereas a fraction ϵ_B of the same goes into generating the small-scale magnetic field that leads to synchrotron cooling. At a given observed time t_{obs} , the emission is obtained by integrating over the equal arrival time surface (EATS). We obtain smoother and more realistic spectral breaks in the comoving spectrum by adopting the smoothing prescription introduced in Granot & Sari (2002) for $k = \{0, 2\}$ and later generalized to $0 \leq k \leq 2$ in Leventis et al. (2012).

We find that the viewing angle of the observer is comparable to the core angle of the energy profile, $\theta_{\text{obs}} \sim \theta_{c, \epsilon}$, which is needed in order to explain the high fluence of the γ -ray emission and the multiwaveband light curve. In contrast to some works (e.g. O’Connor et al. 2023), we find $k \approx 2$ to avoid overproducing the sub-millimetre flux by the FS emission. The kinetic energy of the bipolar outflow in our model is $E_k \propto \theta_F^{2-a} \propto t_{\text{obs}}^{\frac{(2-a)(3-k)}{(8-2k-a)}} \simeq 4.2 \times 10^{52} (t_{\text{obs}}/100 \text{ d})^{0.375}$ erg for no jet break at $t_{\text{obs}} < 100 \text{ d}$ (see Beniamini et al. 2022, for scalings), with $E_{k,\text{max}} \simeq 7 \times 10^{53}$ erg for a maximum jet angular size of $\theta_{\text{max}} = 1 \text{ rad}$. All the model parameters adopted for the FS and RS regions are shown in Table 1. These illustrate one possible approximate solution, while significant degeneracy remains.

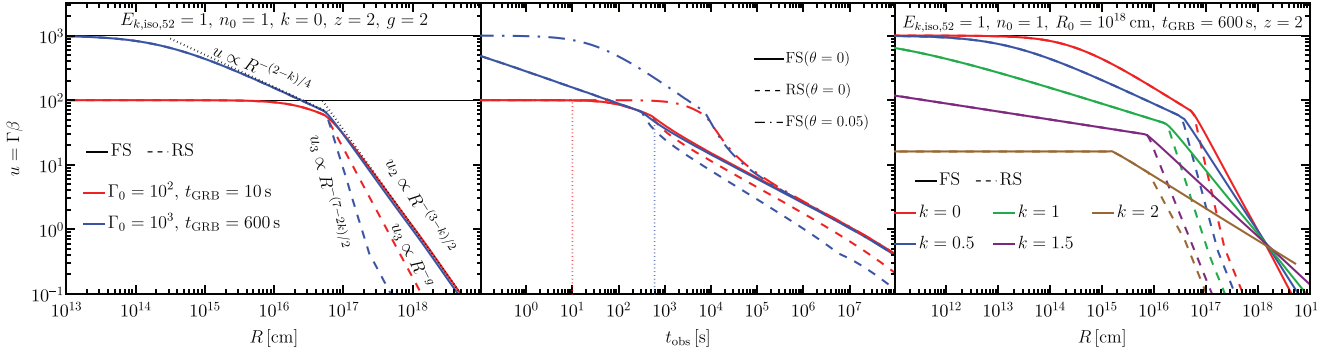


Figure 1. The proper speed $u = \Gamma\beta$ of the shocked regions downstream of the FSs and RSs. *Left:* Two different prompt GRB durations t_{GRB} and initial bulk LFs Γ_0 are chosen to obtain the thin-shell (red) and thick-shell (blue) cases. *Middle:* The same curves from the left-hand panel are now shown as a function of the photon arrival time t_{obs} to an observer at $\theta_{\text{obs}} = 0$ from emission by material moving along different $\theta = \{0, 0.05\}$. The two vertical lines show t_{GRB} (for $\theta = 0$). *Right:* Proper speed evolution in the thick-shell case shown for different external medium density profiles, $n_{\text{ext}} = n_0(R/R_0)^{-k}$ with $\Gamma_0 = 10^3$. The u_3 of the RS-heated material changes slope as it transitions from having a relativistic (thick-shell) to a non-relativistic (thin-shell) temperature.

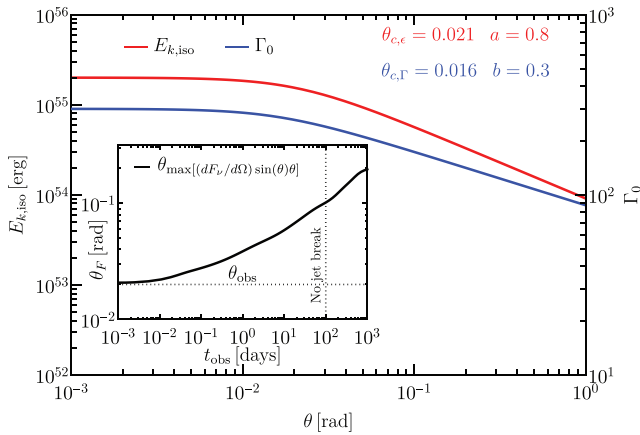


Figure 2. Angular structure of the outflow, showing the isotropic-equivalent (total) kinetic energy and initial bulk LF profiles as a function of polar angle θ measured from the jet symmetry axis. The inset shows the temporal evolution of the polar angle θ_F that dominates the X-ray flux, where the latter has shown no steepening due to a jet break at $t_{\text{obs}} < 100$ d.

The left-hand panel of Fig. 3 compares the model spectra with multiwavelength afterglow observations of GRB 221009A at different times and the right-hand panel shows the corresponding comparison to the light curve. The X-ray afterglow is completely dominated by the FS emission at all times. The optical afterglow is initially RS dominated, at $t_{\text{obs}} \lesssim 0.1$ d, and then becomes increasingly FS dominated. The RS emission also becomes highly suppressed at higher frequencies as the cut-off frequency (ν_{cut}) passes through the optical band towards even lower frequencies over time. The emission is not completely suppressed at $\nu > \nu_{\text{cut}}$, as one would expect from analytic models that only account for emission along the line of sight (LOS). Due to integration over the EATS, high-latitude emission coming from angles $|\theta - \theta_{\text{obs}}| > 1/\Gamma(\theta_{\text{obs}})$ and which was emitted at earlier lab-frame times, when $\nu_{\text{cut}} > \nu$, makes a dominant contribution to the total flux over that emitted along the LOS. This effect will be described in a future publication (Gill & Granot, in preparation).

The middle panel of Fig. 4 compares the model spectra to the radio afterglow data from Laskar et al. (2023). The RS emission clearly dominates the radio flux at all times, with significant FS contribution

to the sub-millimetre flux coming in at late times. The RS radio emission is also self-absorbed below the self-absorption frequency, which decreases with time.

Our model is able to describe the multiwavelength light curve reasonably well. In fact, the FS dominated X-ray light curve compares remarkably well with the data over a wide range of time-scales and captures the shallow break around $t_{\text{br}} \sim 0.8$ d. This break is caused by the shallow break in the energy profile at $\theta \sim 0.04$ rad, emission from which angle dominates the flux at $t_{\text{obs}} = t_{\text{br}}$ (see inset in Fig. 2). A similar conclusion was reached in O’Connor et al. (2023). At $t_{\text{obs}} \lesssim 0.3$ d, $\nu_{\text{opt}} < \nu_m$ and therefore, the FS light curve is expected to be flat when $k = 2$. This means that the slowly decaying optical flux at early times must come from a diminishing RS contribution. The radio data, which is completely dominated by emission from the RS, is explained well by our model at $t_{\text{obs}} \gtrsim 1$ d. At earlier times, it overpredicts the radio flux by a factors of a few when compared with the radio data from Bright et al. (2023). The origin of this discrepancy may lie in the rather coarse exploration of parameter space degeneracies conducted here. This can be addressed more efficiently using a simpler and computationally less intense parametrized model (e.g. Lamb & Kobayashi 2019).

5 CONCLUSIONS

We have explored a potential solution of emission from a jet with a shallow angular profile, both in energy ($a \approx 0.8$) and initial bulk LF ($b \approx 0.3$), to explain the multiwavelength afterglow of the exceptionally bright GRB 221009A. In this model, the radio emission is attributed to that arising from the RS heated ejecta while the optical and X-ray flux is coming from the FS heated external medium.

We find that the data appear to favour that only a small ($\xi_e \approx 10^{-2}$) fraction of shock heated electrons are accelerated to a power-law energy distribution in both shocks. Similar, but somewhat larger, fractions have been obtained in other works (e.g. Salafia et al. 2022) and such a result is consistent with particle-in-cell simulations of magnetized collisionless shocks (Sironi & Spitkovsky 2011).

This is the first GRB in which clear hints for a shallow ($a \lesssim 2$) structured outflow have been found. One of the key observations is the presence of a shallower achromatic break in the light curve ($F_\nu \propto t_{\text{obs}}^a$) with $\Delta\alpha \sim 0.14$ at $t_{\text{obs}} \sim 0.8$ d as compared to $\Delta\alpha = \frac{3-k}{4-k} = 0.75(0.5)$ for $k = 0(2)$, the jet-break expected in a non-spreading sharp-edged jet. O’Connor et al. (2023) pointed out several

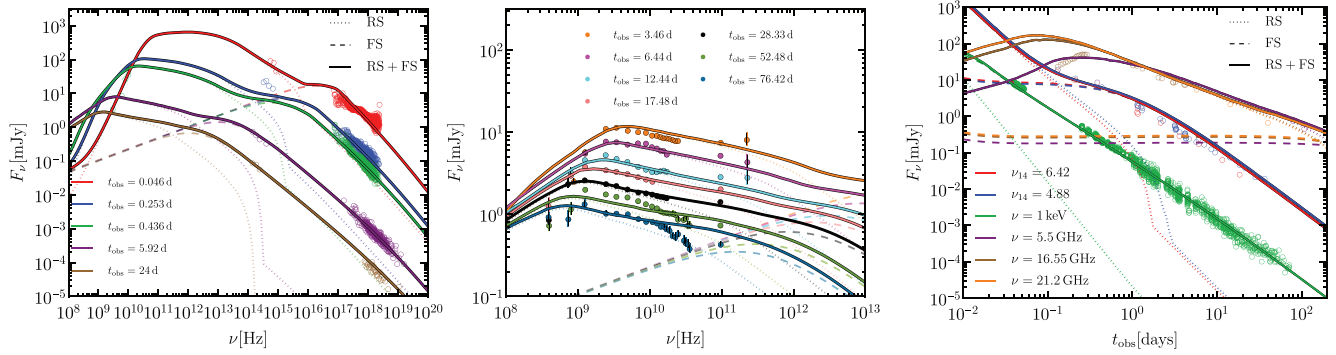


Figure 3. *Left:* Comparison of model spectra with the multiwavelength afterglow of GRB 221009A from radio to X-rays at different observed times t_{obs} (measured from the GRB trigger time). *Middle:* Model comparison to the radio data from Laskar et al. (2023). The total emission is shown with solid lines while the RS and FS components are shown with dotted and dashed lines, respectively. *Right:* Model comparison to the multiwaveband light curve. The X-ray data is from *Swift/XRT*, and the optical and radio data are from Bright et al. (2023) and O’Connor et al. (2023).

Table 1. Model parameters. The external density is normalized at $R_0 = 10^{18}$ cm ($A_* = n_0 R_0^2 / 3 \times 10^{35}$ cm $^{-1}$); $(a, b, \theta_{c,e}, \theta_{c,r}) = (0.8, 0.3, 0.021, 0.016)$.

θ_{obs}	$E_{k,\text{iso,c}}$	Γ_c	$n_0(R_0)$	k	A_*	p_{FS}	$\epsilon_{e,-2}^{\text{FS}}$	$\epsilon_{B,-4}^{\text{FS}}$	$\xi_{e,\text{FS}}$	p_{RS}	$\epsilon_{e,-2}^{\text{RS}}$	$\epsilon_{B,-4}^{\text{RS}}$	$\xi_{e,\text{RS}}$	g	t_{GRB}
0.02 rad	2×10^{55} erg	300	0.1 cm^{-3}	2	0.33	2.4	1.0	1.0	0.01	2.03	8	10	0.01	1.3	500 s

other bright jet-break-less GRBs that may be explained using the model explored here. If true, it may offer strong support for weakly magnetized jets in at least some long–soft GRBs (Bromberg & Tchekhovskoy 2016) as they break out from the stellar envelope, leading to more mixing and a shallow energy angular profile ($a \lesssim 2$).

ACKNOWLEDGEMENTS

RG acknowledges financial support from the UNAM-DGAPA-PAPIIT IA105823 grant, Mexico. JG acknowledges financial support by the ISF-NSFC joint research program (grant no. 3296/19).

DATA AVAILABILITY

The model data can be shared upon reasonable request to the authors.

REFERENCES

- Abbott B. P. et al., 2017, *Phys. Rev. Lett.*, 119, 161101
An Z.-H. et al., 2023, preprint (arXiv:2303.01203)
Beloborodov A. M., Uhm Z. L., 2006, *ApJ*, 651, L1
Beniamini P., Granot J., Gill R., 2020, *MNRAS*, 493, 3521
Beniamini P., Gill R., Granot J., 2022, *MNRAS*, 515, 555
Blandford R. D., McKee C. F., 1976, *Phys. Fluids*, 19, 1130
Bright J. S. et al., 2023, preprint (arXiv:2303.13583)
Bromberg O., Tchekhovskoy A., 2016, *MNRAS*, 456, 1739
Burns E. et al., 2023, *ApJ*, 946, L31
Chiang J., Dermer C. D., 1999, *ApJ*, 512, 699
de Ugarte Postigo A. et al., 2022, GRB Coordinates Network, 32648, 1
Frederiks D. et al., 2023, *ApJ*, 949, L7
Fulton M. D. et al., 2023, *ApJ*, 946, L22
Gill R., Granot J., 2018, *MNRAS*, 478, 4128
Gill R., Granot J., 2020, *MNRAS*, 491, 5815
Gottlieb O., Bromberg O., Singh C. B., Nakar E., 2020, *MNRAS*, 498, 3320
Gottlieb O., Nakar E., Bromberg O., 2021, *MNRAS*, 500, 3511
Granot J., 2005, *ApJ*, 631, 1022
Granot J., 2012, *MNRAS*, 421, 2442
Granot J., Kumar P., 2003, *ApJ*, 591, 1086
Granot J., Ramirez-Ruiz E., 2012, in Kouveliotou C., Woosley S. E., Wijers R. A. M. J., eds, *Gamma-Ray Bursts*. Cambridge Univ. Press, Cambridge, chap. 11 (arXiv:1012.5101)
Granot J., Sari R., 2002, *ApJ*, 568, 820
Granot J., Ramirez-Ruiz E., Perna R., 2005, *ApJ*, 630, 1003
Huang Y. F., Dai Z. G., Lu T., 1999, *MNRAS*, 309, 513
Huang Y., Hu S., Chen S., Zha M., Liu C., Yao Z., Cao Z., Experiment T. L., 2022, GRB Coordinates Network, 32677, 1
Kann D. A. et al., 2023, *ApJ*, 948, L12
Katz J. I., Piran T., 1997, *ApJ*, 490, 772
Kobayashi S., Sari R., 2000, *ApJ*, 542, 819
Kobayashi S., Zhang B., 2003, *ApJ*, 582, L75
Kobayashi S., Piran T., Sari R., 1999, *ApJ*, 513, 669
Kumar P., Granot J., 2003, *ApJ*, 591, 1075
Lamb G. P., Kobayashi S., 2019, *MNRAS*, 489, 1820
Laskar T. et al., 2023, *ApJ*, 946, L23
Lesage S. et al., 2023, preprint (arXiv:2303.14172)
Leventis K., van Eerten H., Meliani Z., Wijers R., 2012, *MNRAS*, 427, 1329
Malesani D. B. et al., 2023, preprint (arXiv:2302.07891)
Margutti R. et al., 2018, *ApJ*, 856, L18
Meszaros P., Rees M. J., 1993, *ApJ*, 405, 278
Nathanail A., Gill R., Porth O., Fromm C. M., Rezzolla L., 2021, *MNRAS*, 502, 1843
Nava L., Sironi L., Ghisellini G., Celotti A., Ghirlanda G., 2013, *MNRAS*, 433, 2107
O’Connor B. et al., 2023, *Sci. Adv.*, 9, eadi1405
Pe’er A., 2012, *ApJ*, 752, L8
Piran T., 1999, *Phys. Rep.*, 314, 575
Racusin J. L. et al., 2008, *Nature*, 455, 183
Rees M. J., Meszaros P., 1992, *MNRAS*, 258, 41
Ren J., Wang Y., Zhang L.-L., Dai Z.-G., 2022, *ApJ*, 947, 53
Ripa J. et al., 2023, *A&A*, preprint (arXiv:2302.10047)
Rossi E., Lazzati D., Rees M. J., 2002, *MNRAS*, 332, 945
Rossi E., Lazzati D., Salmonson J. D., Ghisellini G., 2004, *MNRAS*, 354, 86
Salafia O. S. et al., 2022, *ApJ*, 931, L19
Sari R., 1997, *ApJ*, 489, L37
Sari R., Piran T., 1995, *ApJ*, 455, L143
Sari R., Piran T., 1999a, *ApJ*, 517, L109
Sari R., Piran T., 1999b, *ApJ*, 520, 641

Sato Y., Murase K., Ohira Y., Yamazaki R., 2023, *MNRASL*, 522, L56
Sironi L., Spitkovsky A., 2011, *ApJ*, 726, 75
Troja E. et al., 2019, *MNRAS*, 489, 1919
Williams M. A. et al., 2023, *ApJ*, 946, L24
Yan T., Wei D.-M., Fan Y.-Z., 2007, *Chinese J. Astron. Astrophys.*, 7, 777

Zhang Z.-L., Liu R.-Y., Geng J.-J., Wu X.-F., Wang X.-Y., 2022, *MNRAS*, 513, 4887

This paper has been typeset from a $\text{\TeX}/\text{\LaTeX}$ file prepared by the author.